ELSEVIER

Chemical Engineering Journal 115 (2005) 63–71

Chemical Engineering Journal

www.elsevier.com/locate/cej

Comparative study of oxidative coupling of methane modeling in various types of reactor

Worapon Kiatkittipong [a,b,1], Tomohiko Tagawa [b], Shigeo Goto [b], Suttichai Assabumrungrat [a,*], Kampol Silpasup [a], Piyasan Praserthdam [a]

[a] *Center of Excellence in Catalysis and Catalytic Reaction Engineering, Department of Chemical Engineering, Faculty of Engineering, Chulalongkorn University, Bangkok 10330, Thailand*

[b] *Department of Chemical Engineering, Nagoya University, Chikusa, Nagoya 464-8603, Japan*

Received 18 April 2005; received in revised form 14 August 2005; accepted 27 September 2005

Abstract

Oxidative coupling of methane (OCM) was simulated using plug flow reactor models. Performances of several membrane reactors; i.e. porous membrane reactor (PMR), mixed ionic and electronic conducting membrane reactor (MIEMR) and solid oxide fuel cell reactor (SOFCR) were compared with those of a conventional fixed-bed reactor (FBR). For SOFCR, $La_{0.85}Sr_{0.15}MnO_3$/8 mol%Y_2O_3–ZrO_2/$La_{1.8}Al_{0.2}O_3$ (abbreviated as LSM/YSZ/LaAlO) were the components of cathode, electrolyte and anode, respectively. The membranes for PMR and MIEMR were γ-alumina and $La_{0.40}Sr_{0.60}Ga_{0.40}Fe_{0.60}O_{3-\delta}$, respectively. The kinetic expressions of Li/MgO catalyst were employed in the FBR, PMR and MIEMR models. All types of membrane reactors obviously improved C2 selectivity compared to FBR. However, only SOFCR was inferior to FBR in term of C2 yield due to much lower methane conversion when operating at the same temperature. PMR was superior to the other membrane reactors at low temperature (<1150 K) while MIEMR was attractive at high temperature (>1150 K). However, PMR might not be suitable for use, especially, in the case with inerts or impurities in the oxygen feed. Operation at high pressure was obviously beneficial only to MIEMR and SOFCR. The drawback of PMR was methane loss through the non-selective porous membrane while that of SOFCR was the requirement of higher operating temperature of approximately 200 K compared to the others. However, the electricity simultaneously generated as a by-product might make SOFCR still attractive.

Keywords: Oxidative coupling of methane; Membrane reactor; Solid oxide fuel cell; Comparative simulation

1. Introduction

The conversion of methane into other valuable hydrocarbons has significant industrial importance. Among various schemes for methane conversion, oxidative coupling of methane (OCM) to C2 hydrocarbons (ethane and ethylene) is a promising process to upgrade natural gas. After a pioneer work of Keller and Bhasin [1], there have been extensive research and development efforts in this area. However, the yield of C2 hydrocarbons achieved in a conventional fixed-bed reactor (FBR) was limited to about 25% [2,3] due to the presence of undesired complete oxidation in the gas phase and partially on the catalyst surface.

Applications of membrane reactors to control oxygen concentration along the reactors offer a possibility to achieve much higher C2 hydrocarbons selectivity and yield for OCM. Santamaria and co-workers [4–7] reported that a porous membrane reactor (PMR) gave a considerably better selectivity than FBR; however, the improvement in C2 yield was usually small. Lin and co-workers [8] investigated the performances of OCM reaction in a conventional FBR and a mixed ionic and electronic conducting membrane reactor (MIEMR) packed with Li/MgO catalyst. The kinetic expressions of the reaction over Li/MgO were obtained from their previous work [2]. It was found that the use of MIEMR significantly improved C2 selectivity and yield. They also studied the reaction using a membrane reactor with a catalytically active membrane such as $Bi_{1.5}Y_{0.3}Sm_{0.2}O_{3-\delta}$ (BYS) [9–11] and 25 mol% yttria doped bismuth oxide (BY25) [12]. It was found that the best single-pass C2 yield was achieved in BYS membrane reactor [10]. C2 yield of 35% and C2 selectivity of 54% at 1173 K could be obtained in their system [10].

* Corresponding author. Tel.: +66 2 2186868; fax: +66 2 2186877.
E-mail address: Suttichai.A@chula.ac.th (S. Assabumrungrat).

[1] Nagoya University Program for Academic Exchange (NUPACE)-PhD student supported by AIEJ.

1385-8947/$ – see front matter © 2005 Elsevier B.V. All rights reserved.
doi:10.1016/j.cej.2005.09.018

Nomenclature

a	Knudsen parameter defined in Eq. (2) ($\mathrm{mol\,K^{1/2}\,Pa^{-1}\,m^{-2}\,s^{-1}}$)
b	viscous flow parameter defined in Eq. (2) ($\mathrm{mol\,K\,Pa^{-1}\,m^{-2}}$)
d	thickness of material (m)
F_i	molar flow rate of component i ($\mathrm{mol\,s^{-1}}$)
J_i	molar permeation flux of component i across the membrane ($\mathrm{mol\,m^{-2}\,s^{-1}}$)
L	reactor length (m)
M_i	molecular weight of component i ($\mathrm{kg\,mol^{-1}}$)
P_i	pressure of component i (Pa)
$\mathrm{Per_{O_2}}$	specific oxygen permeability ($\mathrm{mol\,m^{-1}\,s^{-1}}$)
$r_{s,i}$	rate of formation of component i in the shell side ($\mathrm{mol\,m^{-3}\,s^{-1}}$)
$r_{t,i}$	rate of formation of component i in the tube side ($\mathrm{mol\,kg^{-1}\,s^{-1}}$)
R_g	gas constant, 8.314 ($\mathrm{J\,mol^{-1}\,K^{-1}}$)
S	membrane surface area ($\mathrm{m^2}$)
T	temperature (K)
V	volume of reactor ($\mathrm{m^3}$)
W	mass of anode catalyst (kg)
WHSV	weight hour space velocity ($=F_{t,T0}/W$) ($\mathrm{mol\,s^{-1}\,kg^{-1}}$)
x	dimensionless axial length divided by the total length of reactor
y_I	mole fraction of inert at the feed

Greek letters

γ	molar flow rate ratio ($=F_i/F_{T0}$)
μ	viscosity of gas mixture (Pa s)

Subscripts

i	component i
s	shell side
t	tube side
T	total
0	feed

Some researchers employed a solid oxide fuel cell reactor (SOFCR) for the electrochemical selective oxidation of methane to C2 hydrocarbons [13–15]. Electric power was generated simultaneously with the selective production of C2 hydrocarbons. In our previous papers, OCM was studied in SOFCR. Particular focuses were on catalyst preparation methods [15–18] and reactor performance test [13,15,19]. The fuel cell type-temperature-programmed desorption (FC-TPD) technique was proposed to investigate types of oxygen species under the fuel cell operation [20]. The knowledge of oxygen species from FC-TPD [19–21] and the oxygen permeation through LSM/YSZ/LaAlO [22] were taken into account to obtain the kinetic parameters of the reactions on the anode [15]. A set of the kinetic expressions using two different oxygen species; i.e. oxygenate and coupling species, was useful to evaluate OCM in a tubular SOFCR. The SOFCR for OCM was considered as a good reactor for C2 production although the obtained electricity was quite far from a typical SOFC [23].

Nowadays, mixed ionic and electronic conductors with high oxygen permeability have been developed, offering an opportunity for use in a membrane reactor. Perovskite-type (A, La)(Co, Fe)$O_{3-\delta}$ membranes (where A is alkaline-earth element) are among the well-known mixed conductors with the highest oxygen permeability; however, most of them are thermodynamically and/or dimensionally unstable under large oxygen chemical potential gradient typically encountered in membrane reactor operating conditions [24,25]. At temperatures below 1000–1070 K, the membrane performance is degraded with time. Moreover, it possesses a very high thermal expansion property [24,25]. One alternative group of the membrane materials is a $LaGaO_3$-based mixed conductor with perovskite-type structure. Substitution of La with alkaline-earth cations (Sr, Ca, Ba) and Ga with bivalent cations (Mg, Ni) results in high ionic conduction. One of the highest oxygen ionic conductor is a La(Sr)Ga(Mg)$O_{3-\delta}$ (LSGM) solid solution [25,26]. Even though the use of this conductor in MIEMR is less complicated than SOFCR, no electricity is obtained as a by-product unlike SOFCR.

Concerning simulation works, Santamaria et al. [27] proposed a new distributed oxygen feed between a series of packbed reactors. C2 yield of 29% and C2 selectivity of 76% were obtained. Cheng and Shuai [28] simulated OCM in a plug flow reactor using lead oxide catalyst impregnated on γ-alumina. The kinetic equations of OCM with PbO/Al_2O_3 catalyst obtained by Hinsen et al. [29] were used in their work. Their simple model assumed non-homogeneous gas phase reaction, uniform permeation pattern and no permeation of other components through the membrane except oxygen. Coronas et al. [30] investigated the membrane activity on the performance of a catalytic membrane reactor. A commercial γ-alumina membrane (Membralox, SCT) was used as the starting material for the catalytic membrane preparation. Silica was deposited inside the membrane, in order to reduce the initial porosity, and to obtain an appropriate permeation flux. Solution of lithium carbonate or sodium carbonate was impregnated to reduce the surface acidity. The model was developed considering a gas phase reaction and catalytic activity of the modified membrane. Although, it is generally accepted that the membrane reactors for OCM are superior to the conventional FBR, comparison between various membrane reactor configurations has not been performed simultaneously.

It is, therefore, the objective of this paper to compare performances of PMR, MIEMR and SOFCR for OCM to C2 hydrocarbons. Kinetic expressions of Li/MgO catalyst [8] and permeation equations of gases through a commercial "Membralox" membrane with 10 nm pore size [31] and "$La_{0.40}Sr_{0.60}Ga_{0.40}Fe_{0.60}O_{3-\delta}$" mixed conductor [25] were used for modeling FBR, PMR and MIEMR. Our previous model [15,22] was used to simulate the $La_{0.85}Sr_{0.15}MnO_3$/8 mol% Y_2O_3–ZrO_2/$La_{1.8}Al_{0.2}O_3$ (abbreviated as LSM/YSZ/LaAlO) SOFCR. The obtained C2 selectivity and yield of the different reactors were compared under different operating conditions.

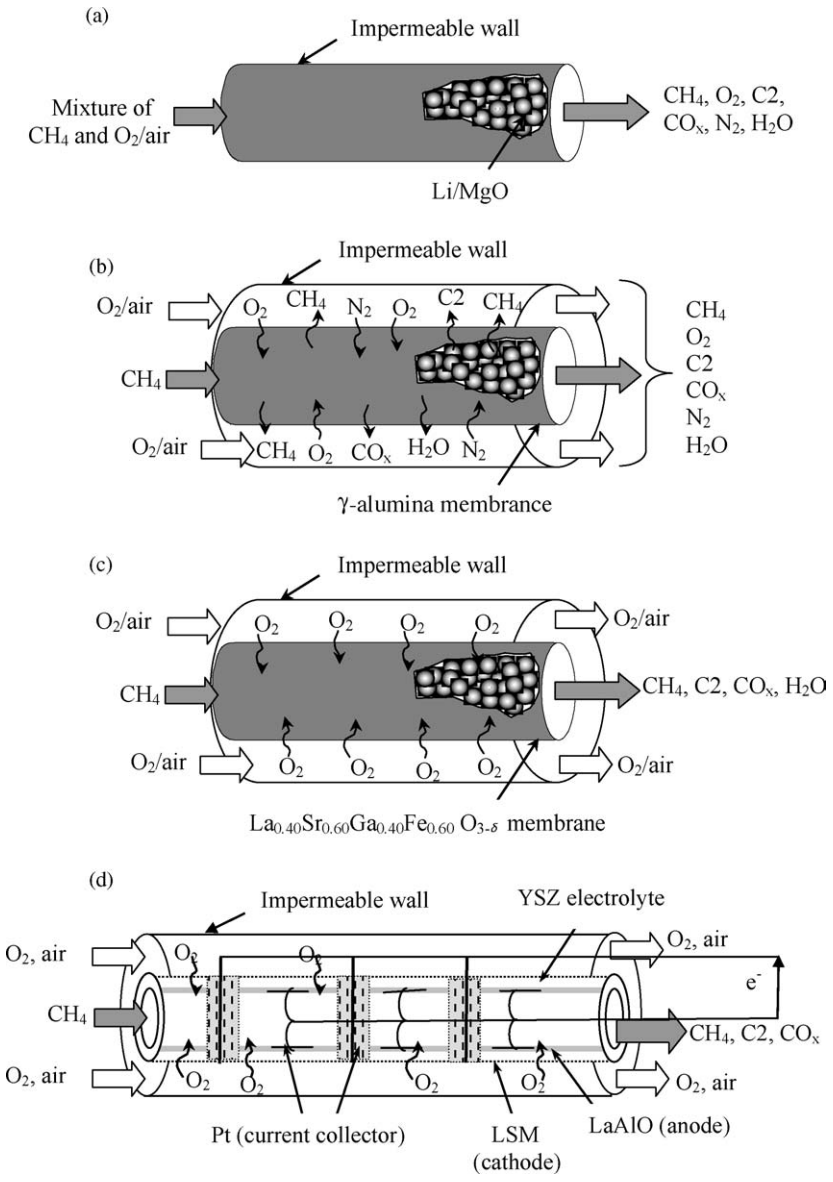

Fig. 1. Proposed schemes for various OCM reactors: (a) FBR, (b) PMR, (c) MIEMR and (d) SOFCR.

2. Modeling

Fig. 1(a) shows the scheme of FBR. Methane, oxygen/air and inert gas were mixed and co-fed to an impermeable tubular reactor. The membrane reactors in this study are double tubular reactors as shown in Fig. 1(b)–(d). The inner tube is made of a porous γ-alumina membrane, a dense $La_{0.40}Sr_{0.60}Ga_{0.40}Fe_{0.60}O_{3-\delta}$ membrane and an LSM/YSZ/LaAlO cell for PMR, MIEMR and SOFCR, respectively. The outer shell is an impermeable wall. The simulations were carried out using a reactor length of 20 cm, an inner diameter of the inner tube of 1.8 cm and an inner diameter of the shell tube of 4 cm.

2.1. Mass balance equations

By assuming plug flow and isothermal conditions, the mass balance equation of the tube side for PMR, MIEMR, SOFCR and also FBR, which has only one tube is given as:

$$\frac{d\gamma_{t,i}}{dx} = \left\{ r_{t,i} + \left(\frac{S}{W}\right) J_i \right\} \frac{W}{F_{t,T0}} \quad (1)$$

At the entrance ($x = 0$), $\gamma_{t,CH_4} = F_{t,CH_40}/F_{t,T0}$, $\gamma_{t,i} = 0$ (products).

The mass balance equation in the shell side is given as:

$$\frac{d\gamma_{s,i}}{dx} = \left\{ r_{s,i} - \left(\frac{S}{V}\right) J_i \right\} \frac{V}{F_{s,T0}} \quad (2)$$

At the entrance ($x = 0$), $\gamma_{s,O_2} = F_{s,O_20}/F_{s,T0}$, $\gamma_{s,i} = 0$ (products).

2.2. Permeation equations

For FBR, the permeation rate of component i is zero ($J_i = 0$) because the tube is made of an impermeable wall. Oxygen/air is co-fed with the methane feed in the tube.

For PMR, all of component i can permeate through the membrane because the γ-alumina membrane is not highly selective. The permeation data for PMR is based on the permeation data of gases through a commercial "Membralox" membrane. The membrane consists of porous α-alumina supports and a separative layer of γ-alumina with a pore size of 1×10^{-8} m and a thickness of 5×10^{-6} m. Both Knudsen and viscous flow mechanisms are important and can be expressed as follows [31,32]:

$$J_i = \frac{a}{\sqrt{M_i T}}(P_{s,i} - P_{t,i}) + \frac{b}{2\mu T}(P_{s,i}^2 - P_{t,i}^2) \quad (3)$$

where

$$a = 2.298 \times 10^{-4}\ \text{mol K}^{1/2}\ \text{Pa}^{-1}\ \text{m}^{-2}\ \text{s}^{-1} \quad (4)$$

$$b = 4.779 \times 10^{-14}\ \text{mol K Pa}^{-1}\ \text{m}^{-2} \quad (5)$$

The gas viscosity can be estimated by Wilke's correlation [33].

For MIEMR, the permeation rate of component i except oxygen is zero ($J_i = 0$) due to the highly selective property of the membrane. The oxygen permeation rate through the $La_{0.40}Sr_{0.60}Ga_{0.40}Fe_{0.60}O_{3-\delta}$ mixed ionic and electronic conductor with a thickness (d) of 1×10^{-4} m is expressed as follows [25]:

$$J_{O_2} = \frac{\text{Per}_{O_2}}{d} \ln\left(\frac{P_{s,O_2}}{P_{t,O_2}}\right) \quad (6)$$

where

$$\text{Per}_{O_2} = 0.0645 \exp\left(\frac{-108\,400}{R_g T}\right) \quad (7)$$

The value of Per_{O_2} of $La_{0.40}Sr_{0.60}Ga_{0.40}Fe_{0.60}O_{3-\delta}$ membrane was determined from Fig. 6 of Ref. [25].

For SOFCR, the permeation rate of component i except oxygen is zero ($J_i = 0$) due to the highly selective property of the membrane. The oxygen permeation rate through the LSM/YSZ/LaAlO SOFCR can be estimated from our previous model [22]. The thickness of YSZ membrane was 1.5×10^{-3} m in this study.

2.3. Kinetic rate expressions

2.3.1. Tube side reactions

Li/MgO catalyst was placed in the tube side of FBR, PMR and MIEMR. The solid density of catalyst with the size of 100–200 μm is about 2022 kg m^{-3} [34] and the void fraction of 0.34 was assumed [35]. The kinetic expressions of the reactions on the Li/MgO catalyst were obtained from Kao et al. [8]. For LSM/YSZ/LaAlO SOFCR, the reaction rate expressions were provided in our previous work [15].

2.3.2. Shell side reactions

There was no catalyst in the shell side. The homogeneous gas phase reaction rate on the shell side ($r_{s,i}$) was cited from Lane and Wolf [36].

The partial pressures in the tube side and the shell side can be determined as follows:

$$P_{t,i} = \frac{P_{t,T}\gamma_{t,i}}{\sum \gamma_{t,i}} \quad (8)$$

$$P_{s,i} = \frac{P_{s,T}\gamma_{s,i}}{\sum \gamma_{s,i}} \quad (9)$$

The simulations were performed by using an all-purpose equation solver, EQUATRAN-G (Omega Simulation, Japan). FBR and SOFCR models were verified by comparing the simulation results with experimental results of Kao et al. [8] and our previous results [15,23]. Good agreements were observed for both cases.

It should be noted that for simplicity the isothermal condition and negligible radial and axial diffusion effects were assumed in this study. Due to the exothermic nature of OCM, the hot spot temperature may be observed particularly with FBR. However, the hot spot problem is less severe for the membrane reactors with the distributed oxygen supply along the reactors. Therefore, the reactors can be maintained at a nearly isothermal condition. The isothermal behavior of PMR and SOFCR has been reported in the literature [23,37,38]. The radial diffusion could be neglected because of small bed diameter [39,40] and the effect of axial diffusion becomes negligible when the reactor is operated under the turbulent flow regime [40,41]. It is further assumed that the catalytic activity of the membrane is negligible. This assumption for the γ-alumina porous membranes has been made by a number of previous works on oxidative dehydrogenations of ethane [42], propane [43] and *n*-butane [44,45] and also on OCM reaction [4,5,28,46]. However, no literature has reported the activity of the $La_{0.40}Sr_{0.60}Ga_{0.40}Fe_{0.60}O_{3-\delta}$ membrane on OCM.

In this study, the feed molar flow rates of methane, oxygen and inert gas are the same for FBR, PMR and MIEMR for each simulation condition. For SOFCR, the amount of catalyst is not the same as the others; however, WHSV and methane to oxygen ratio of all simulation are fixed at 1.8×10^{-3} mol s^{-1} kg^{-1} and 2.0, respectively.

3. Results and discussion

3.1. Characteristics of different reactors

The characteristics of different reactors for OCM were investigated. Li/MgO OCM catalysts are packed in FBR, PMR and MIEMR while LaAlO is used as the anode catalyst for SOFCR. Mole fraction of methane: oxygen: inert in feed of 0.3:0.15:0.55 and WHSV of 1.8×10^{-3} mol s^{-1} kg^{-1} are maintained for all simulations. The temperatures of FBR, PMR and MIEMR are considered at 1073 K while at 1273 K for SOFCR; the reason will be discussed in the following section.

Fig. 2 shows methane and oxygen conversions along the reactor length for various types of reactor. It is worth to note that oxygen is completely consumed within the initial part of FBR, while at the same oxygen feed flow rate, it is enough to supply along the reactor for the other membrane reactors. This results in

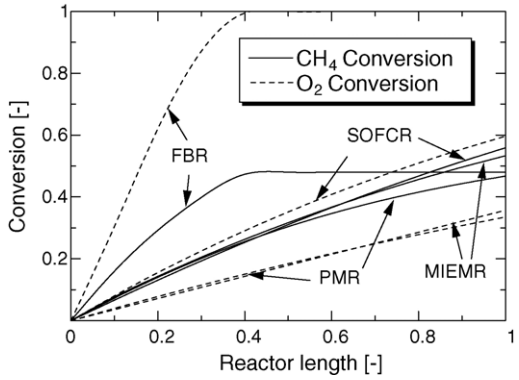

Fig. 2. Methane and oxygen conversions along the reactor length for various types of reactor (WHSV = 1.8×10^{-3} mol s^{-1} kg^{-1}, $L = 0.2$ m, $P_{t,T} = P_{s,T} = 1.013 \times 10^5$ Pa, methane (in the tube side):oxygen (in the shell side):inert (in the shell side) = 0.3:0.15:0.55, $T = 1073$ K for FBR, PMR and MIEMR, and $T = 1273$ K for SOFCR).

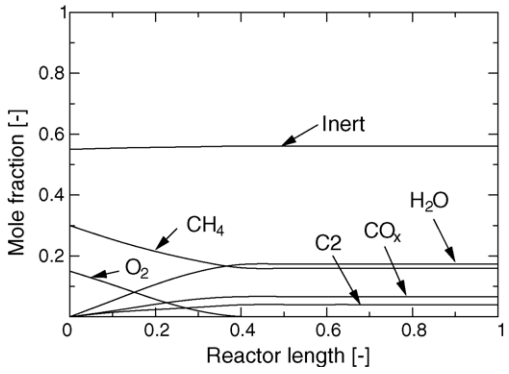

Fig. 4. Mole fraction profiles with reactor length of FBR (WHSV = 1.8×10^{-3} mol s^{-1} kg^{-1}, $L = 0.2$ m, $P_{t,T} = P_{s,T} = 1.013 \times 10^5$ Pa, methane (in the tube side):oxygen (in the shell side):inert (in the shell side) = 0.3:0.15:0.55, $T = 1073$ K).

an increase of C2 yield with increasing reactor length for all of membrane reactors as shown in Fig. 3. It should be pointed out that C2 selectivity is the highest at the reactor inlet and sharply decreases in the case of FBR while slightly decreases in the case of PMR. For MIEMR and SOFCR, C2 selectivities are almost constant along the reactor. To understand this behavior, mole fraction profiles were plotted. For FBR as shown in Fig. 4, CO_x increases more than C2 along the reactor and becomes constant after oxygen is completely consumed. Since FBR gives lower C2 selectivity than other membrane reactors (Fig. 3), the oxygen consumption is higher (Fig. 2) in order to produce CO and CO_2 by the reaction of:

$$CH_4 + \left(\frac{x}{2} + 1\right) O_2 \rightarrow CO_x + 2H_2O$$

Compared between membrane reactors, PMR gives lower methane conversion and C2 yield than MIEMR and SOFCR (Figs. 2 and 3). Mole fraction profiles in both shell and tube sides in PMR are provided as shown in Fig. 5. Solid lines and dashed lines are the simulation results considering and not considering homogeneous gas phase reaction on the shell side, respectively. Almost the same results are obtained. These indicate that lower C2 yield obtained in PMR is not affected by homogeneous gas phase reaction on the shell side. On the contrary, since the porous membrane is not highly selective membrane, not only methane loss to shell side that makes low methane conversion but also the permeation of inert from the shell side to the tube side which makes low reaction rate. However, homogeneous gas phase reactions on the shell side are still included in our models in the following sections.

Mole fraction profiles of MIEMR and SOFCR are shown in Figs. 6 and 7, respectively. No reactant and product losses to the shell side occur because only oxygen permeates selectively through membranes in both cases. It should be noted that oxygen

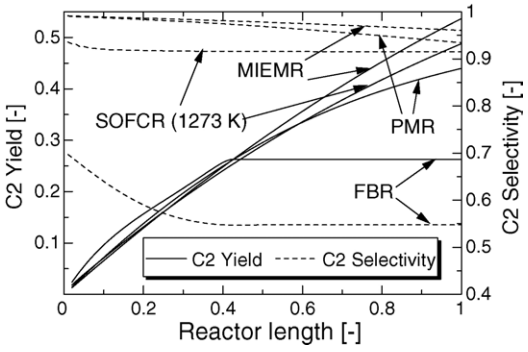

Fig. 3. C2 yield and C2 selectivity along the reactor length for various types of reactor (WHSV = 1.8×10^{-3} mol s^{-1} kg^{-1}, $L = 0.2$ m, $P_{t,T} = P_{s,T} = 1.013 \times 10^5$ Pa, methane (in the tube side):oxygen (in the shell side):inert (in the shell side) = 0.3:0.15:0.55, $T = 1073$ K for FBR, PMR and MIEMR, and $T = 1273$ K for SOFCR).

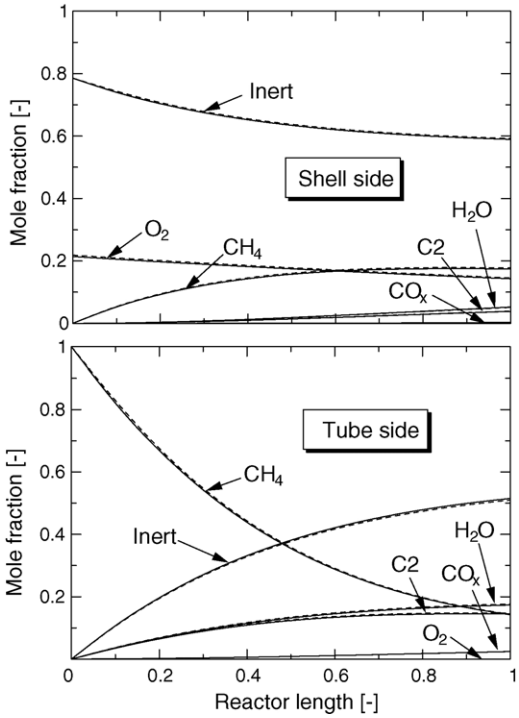

Fig. 5. Mole fraction profiles with reactor length of PMR (WHSV = 1.8×10^{-3} mol s^{-1} kg^{-1}, $L = 0.2$ m, $P_{t,T} = P_{s,T} = 1.013 \times 10^5$ Pa, methane (in the tube side):oxygen (in the shell side):inert (in the shell side) = 0.3:0.15:0.55, $T = 1073$ K).

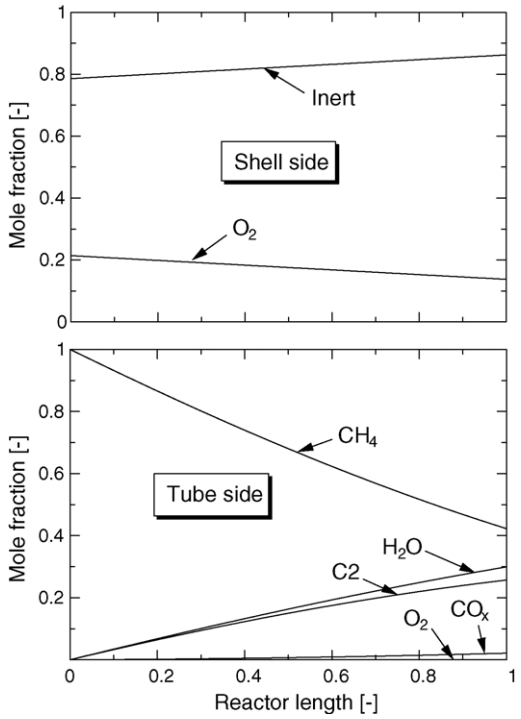

Fig. 6. Mole fraction profiles with reactor length of MIEMR (WHSV = 1.8×10^{-3} mol s^{-1} kg^{-1}, $L = 0.2$ m, $P_{t,T} = P_{s,T} = 1.013 \times 10^5$ Pa, methane (in the tube side):oxygen (in the shell side):inert (in the shell side) = 0.3:0.15:0.55, $T = 1073$ K).

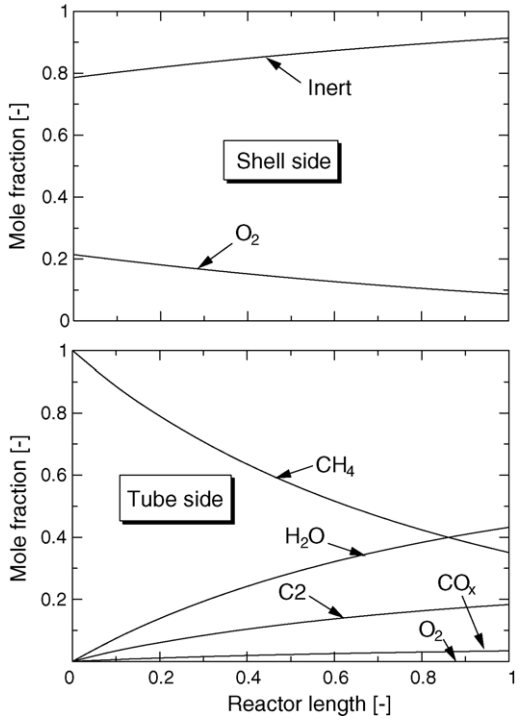

Fig. 7. Mole fraction profiles with reactor length of SOFCR (WHSV = 1.8×10^{-3} mol s^{-1} kg^{-1}, $L = 0.2$ m, $P_{t,T} = P_{s,T} = 1.013 \times 10^5$ Pa, methane (in the tube side):oxygen (in the shell side):inert (in the shell side) = 0.3:0.15:0.55, $T = 1273$ K).

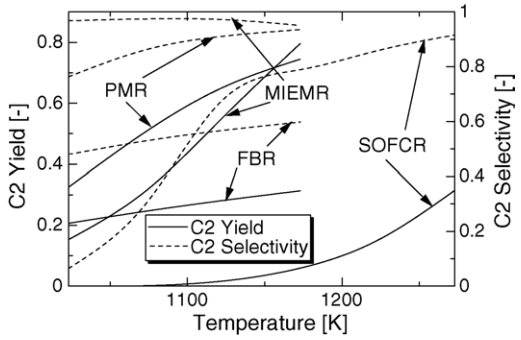

Fig. 8. Effect of temperature on C2 yield and C2 selectivity for various types of reactor ($y_I = 0$, WHSV = 1.8×10^{-3} mol s^{-1} kg^{-1}, $L = 0.2$ m and $P_{t,T} = P_{s,T} = 1.013 \times 10^5$ Pa).

consumption in the case of SOFCR, which is much larger than PMR and MIEMR (Fig. 2) is dominated from further reaction of ethane to ethylene:

$$C_2H_6 + \tfrac{1}{2}O_2 \rightarrow C_2H_4 + H_2O$$

Even though different types of membrane give different reactor characteristics and performances, it should be noted that the membrane reactor could distribute oxygen feed and keep low oxygen partial pressure in the reaction side (as shown in Figs. 5–7), leading to high C2 selectivity.

3.2. Effect of operating temperature

Fig. 8 shows the effect of temperature on C2 yield and C2 selectivity of various types of reactors. Pure methane and oxygen are fed with a molar ratio of 2.0. The temperatures of FBR, PMR and MIEMR are considered in a range of 1023–1173 K, corresponding to the validation limit of the kinetic expressions [8]. C2 yield and C2 selectivity increase with increasing temperature for all reactors. It is obvious that both PMR and MIEMR give higher C2 yield and C2 selectivity than FBR as expected. It should be noted that for the case with pure oxygen feed in the shell side, methane conversion of PMR is higher than that of MIEMR especially at temperature lower than 1150 K (the results are not shown) because of higher oxygen permeability. On the other hand, C2 selectivity of PMR is lower than MIEMR because the decrease of methane partial pressure in the tube side due to methane loss leads to low methane and oxygen ratio, which is not favorable. Even though C2 selectivity in SOFCR dramatically increases with increasing temperature, C2 yield is very low. This suggests that SOFCR should be operated at higher temperature than the others in order to obtain enough oxygen permeability. Our previous work suggested that our SOFCR system was a good reactor for C2 production where electric power was generated simultaneously [23]. The high temperature requirement may be the main disadvantage of SOFCR; however, the electricity, which is simultaneously generated, may compensate and make SOFCR still attractive. From this reason, SOFCR was simulated at higher temperature than the others in the previous section and also the following sections.

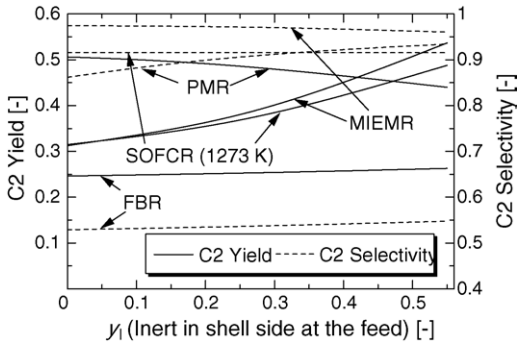

Fig. 9. Effect of inert mole fraction in shell side at the feed on C2 yield and C2 selectivity for various types of reactor (WHSV = 1.8×10^{-3} mol s^{-1} kg^{-1}, $L = 0.2$ m, $P_{t,T} = P_{s,T} = 1.013 \times 10^5$ Pa, $T = 1073$ K for FBR, PMR and MIEMR, and $T = 1273$ K for SOFCR).

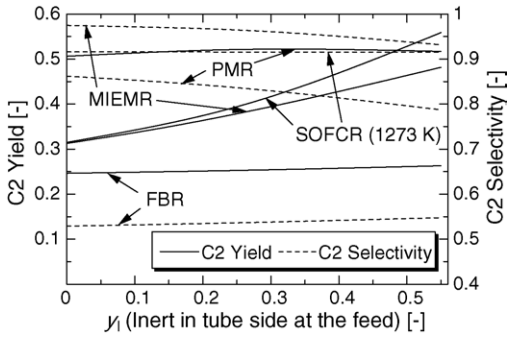

Fig. 10. Effect of inert mole fraction in tube side at the feed on C2 yield and C2 selectivity for various types of reactor (WHSV = 1.8×10^{-3} mol s^{-1} kg^{-1}, $L = 0.2$ m, $P_{t,T} = P_{s,T} = 1.013 \times 10^5$ Pa, $T = 1073$ K for FBR, PMR and MIEMR, and $T = 1273$ K for SOFCR).

3.3. Effect of inert mole fraction at the feed

According to a viewpoint of the oxygen purification cost, air is considered to use as an oxidant in the system. Methane and oxygen feeds are kept at a mole ratio of 2.0 and WHSV is maintained at 1.8×10^{-3} mol s^{-1} kg^{-1} for all simulations. The inert mole fraction in the shell side at the feed was increased from 0 to 0.55, corresponding to mole fraction of methane:oxygen:inert as 0.667:0.333:0 for pure oxygen feed and 0.3:0.15:0.55 for air feed. In the case of FBR, inert was mixed and co-fed with methane and oxygen. As shown in Fig. 9, the increase in the inert mole fraction does not significantly affect C2 selectivity. Even though, methane residence time increases with increasing inert mole fraction at the feed, methane conversion may not be improved because of insufficient oxygen supply, and therefore, C2 yield only slightly increases.

For the membrane reactors, the oxygen partial pressure in the shell side is decreased with increasing inert mole fraction and thus decreases the driving force for the oxygen permeation. It results in high methane and oxygen molar ratio in the reactor side, which leads to higher C2 selectivity as shown in PMR case. However, when oxygen permeation decreases, the overall reaction rate decreases. In addition, even though the residence time increases with decreasing methane feed flow rate, methane conversion may not be efficiently improved because of the significant loss of methane to the shell side in the case of PMR. This suggested that the porous membrane might not be suitable for use in the membrane reactor especially in the case of inerts or impurities in the oxygen feed.

For MIEMR case, the increase in the inert mole fraction in the shell side is insignificantly affected C2 selectivity. Since there is no methane loss to the shell side, methane can be converted more completely with increasing the residence time. It results in the increase of C2 yield. The same results are also observed in SOFCR case. However, it should be noted that SOFCR was simulated at 1273 K, which was 200 K higher than the other cases.

The effect of inert mole fraction at the feed on reactor performance was extended to the case of diluted reactant in the tube side. Pure oxygen was fed to the shell side of reactors. Fig. 10 shows the reactor performances at various values of inert mole fraction in the tube side at the feed. In PMR case, as the inert mole fraction in the tube side increases, the partial pressure of methane decreases and then C2 selectivity decreases. However, it results in reduction of methane loss to the shell side. These effects make C2 yield to be traded off and shown some optimum conditions. The mole fraction profiles of each species of PMR are shown as solid lines, methane and oxygen conversion as dashed line in Fig. 11. Comparison between two cases with the inert feed in the shell and the tube sides at $y_I = 0.55$ as shown in Figs. 2 and 11, respectively, reveals that oxygen conversion increased rapidly when changing inert feed from the shell side to the tube side due to the increased oxygen feed concentration which increases the driving force of oxygen permeation. Since the oxygen permeation increases, the methane conversion also increases.

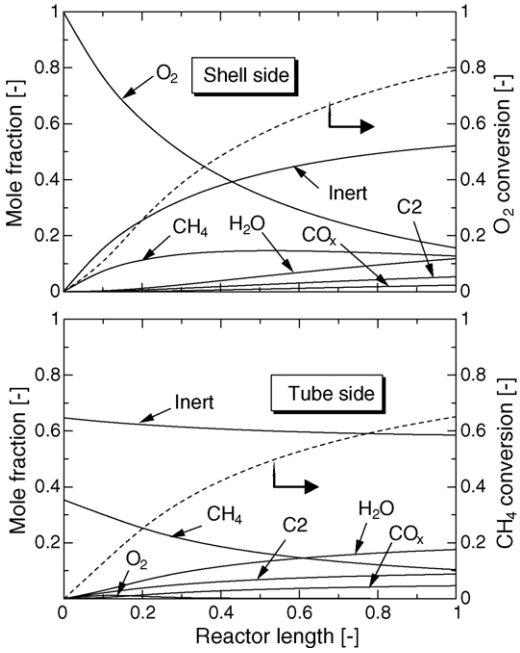

Fig. 11. Mole fraction profiles, methane and oxygen conversions with reactor length of PMR (WHSV = 1.8×10^{-3} mol s^{-1} kg^{-1}, $L = 0.2$ m, $P_{t,T} = P_{s,T} = 1.013 \times 10^5$ Pa, methane (in the tube side):oxygen (in the shell side):inert (in the tube side) = 0.3:0.15:0.55, $T = 1073$ K).

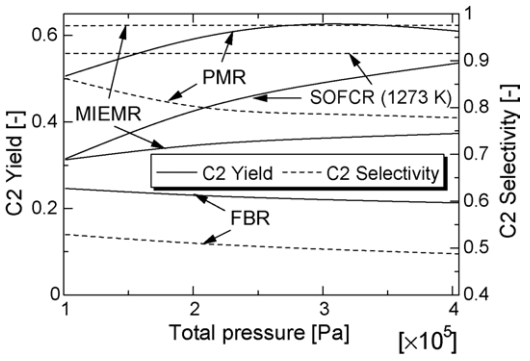

Fig. 12. Effect of operating pressure on C2 yield and C2 selectivity ($y_I = 0$, WHSV = 1.8×10^{-3} mol s^{-1} kg^{-1}, $L = 0.2$ m, $T = 1073$ K for FBR, PMR and MIEMR, and $T = 1273$ K for SOFCR).

For MIEMR case, the effect of increase of residence time which leads to higher methane conversion plays more important role than the effect of reduction of methane partial pressure which leads to the decrease of C2 selectivity as shown in Fig. 10. Consequently, the increase of C2 yield is obtained. Similar tendency can be observed for SOFCR case. It should be pointed out in this section that C2 yield usually increases with increasing residence time (as shown in Figs. 9 and 10) in MIEMR and SOFCR cases; however, it may not increase in FBR and PMR cases.

3.4. Effect of operating pressure

Effect of operating pressure on the performances of the reactors was studied. In order to avoid cell damages, the pressures in both shell and tube sides are maintained at the same value in the cases of PMR, MIEMR and SOFCR. The results shown in Fig. 12 indicate that C2 yield increases with increasing operating pressure for all types of reactor except FBR. For the membrane reactors, as the operating pressure increases, the driving force for the oxygen permeation through the membrane increases. This tendency can be explained by the increase of oxygen partial pressure in the shell side and also the acceleration of the reaction rate by the increased methane partial pressure. However, in the cases of FBR and PMR whose C2 selectivity strongly depends on partial pressure of methane and oxygen, C2 selectivity decreases with increasing operating pressure. C2 yield in the case of PMR shows trade off between the increase in methane conversion and the decrease in C2 selectivity with increasing operating pressure. From the results, the operation at high pressure is obviously beneficial to MIEMR and SOFCR; however, other considerations such as problems on seals and mechanical properties of the oxide conductor should be taken into account for selecting a suitable operating pressure.

4. Conclusion

Plug flow reactor models were used to compare the performances of the membrane reactors, i.e. porous membrane reactor (PMR), mixed ionic and electronic conducting membrane reactor (MIEMR) and solid oxide fuel cell reactor (SOFCR) with those of the conventional fixed-bed reactor (FBR) on the oxidative coupling of methane (OCM) for C2 hydrocarbons production. It was found that FBR was not recommended for OCM while PMR and MIEMR were suitable at temperatures lower than 1150 K and higher than 1150 K, respectively. However, the use of PMR is not recommended for in the case of air feed or oxygen feed with impurities. Operation at high pressure was beneficial only to MIEMR and SOFCR. The drawback of PMR was the methane loss through the non-selective porous membrane while that of SOFCR was the requirement of higher operating temperature of approximately 200 K compared to the others. However, the electricity simultaneously generated as a by-product might make SOFCR still attractive.

Acknowledgements

The authors gratefully acknowledged the supports from The Thailand Research Fund (TRF), TJTTP-JBIC and NUPACE. A part of this study was also supported by a Grant-in-aid for Scientific Research and Graduate School of Chulalongkorn University.

References

[1] G.E. Keller, M.M. Bhasin, J. Catal. 73 (1982) 9–19.
[2] W. Wang, Y.S. Lin, J. Membr. Sci. 103 (1995) 219–233.
[3] J.H. Lunsford, Catal. Today 63 (2000) 165–174.
[4] J. Coronas, M. Menendez, J. Santamaria, Chem. Eng. Sci. 49 (1994) 2015–2025.
[5] D. Lafarga, J. Santamaria, M. Menendez, Chem. Eng. Sci. 49 (1994) 2005–2013.
[6] J. Coronas, M. Menendez, J. Santamaria, Chem. Eng. Sci. 49 (1994) 4749–4757.
[7] J. Herguido, D. Lafarga, M. Menendez, J. Santamaria, C. Guimon, Catal. Today 25 (1995) 263–269.
[8] Y.K. Kao, L. Lei, Y.S. Lin, Ind. Eng. Chem. Res. 36 (1997) 3583–3593.
[9] F.T. Akin, Y.S. Lin, Y. Zeng, Ind. Eng. Chem. Res. 40 (2001) 5908–5916.
[10] F.T. Akin, Y.S. Lin, AIChE J. 48 (2002) 2298–2306.
[11] Y. Zeng, Y.S. Lin, AIChE J. 47 (2001) 436–444.
[12] Y. Zeng, Y.S. Lin, J. Catal. 193 (2000) 58–64.
[13] T. Tagawa, K.K. Moe, M. Ito, S. Goto, Chem. Eng. Sci. 54 (1999) 1553–1557.
[14] X.M. Guo, K. Hidajat, C.B. Ching, Catal. Today 50 (1999) 109–116.
[15] W. Kiatkittipong, T. Tagawa, S. Goto, S. Assabumrungrat, P. Praserthdam, J. Chem. Eng. Jpn. 37 (2004) 1461–1470.
[16] K.K. Moe, T. Tagawa, S. Goto, J. Ceram. Soc. Jpn. 106 (1998) 242–247.
[17] K.K. Moe, T. Tagawa, S. Goto, J. Ceram. Soc. Jpn. 106 (1998) 754–758.
[18] A.S. Carrillo, T. Tagawa, S. Goto, Mater. Res. Bull. 36 (2001) 1017–1027.
[19] T. Tagawa, K.K. Moe, T. Hiramatsu, S. Goto, Solid State Ionics 106 (1998) 227–235.
[20] W. Kiatkittipong, T. Tagawa, S. Goto, S. Assabumrungrat, P. Praserthdam, Solid State Ionics 166 (2004) 127–136.
[21] T. Tagawa, K. Kuroyanagi, S. Goto, S. Assabumrungrat, P. Praserthdam, Chem. Eng. J. 93 (2003) 3–9.
[22] W. Kiatkittipong, T. Tagawa, S. Goto, S. Assabumrungrat, P. Praserthdam, Chem. Eng. J. 106 (2005) 35–42.
[23] W. Kiatkittipong, S. Goto, T. Tagawa, S. Assabumrungrat, P. Praserthdam, J. Chem. Eng. Jpn., in press.
[24] V.V. Kharton, A.A. Yaremchenko, A.V. Kovalevsky, A.P. Viskup, E.N. Naumovich, P.F. Kerko, J. Membr. Sci. 163 (1999) 307–317.

[25] A.L. Shaula, A.A. Yaremchenko, V.V. Kharton, D.I. Logvinovich, E.N. Naumovich, A.V. Kovalevsky, J.R. Frade, F.M.B. Marques, J. Membr. Sci. 221 (2003) 69–77.
[26] T. Ishihara, H. Matsuda, Y. Takita, Solid State Ionics 79 (1995) 147–151.
[27] J. Santamaria, M. Menendez, J.A. Pena, J.I. Barahona, Catal. Today 13 (1992) 353.
[28] S. Cheng, X. Shuai, AIChE J. 41 (1995) 1598–1601.
[29] W. Hinsen, W. Bytyn, M. Baerns, Proc. Int. Cong. Catal. Germany 3 (1984) 581.
[30] J. Coronas, A. Gonzola, D. Lafarga, M. Menendez, AIChE J. 43 (1997) 3095–3104.
[31] S. Assabumrungrat, D.A. White, Chem. Eng. Sci. 51 (1996) 5241–5250.
[32] S. Assabumrungrat, Mechanisms and modelling of gas separations through ceramic membrane in chemical reaction processes, PhD Thesis, London, 1996.
[33] R.B. Bird, W.E. Steward, E.N. Lightfoot, Transport Phenomena, Wiley, New York, 1960.
[34] E. Marco, A. Santos, M. Menendez, J. Santamaria, Powder Tech. 92 (1997) 47–52.
[35] W.L. McCabe, J.C. Smith, P. Harriott, Unit Operations of Chemical Engineering, McGraw-Hill, Singapore, 2001.
[36] G.S. Lane, E.E. Wolf, J. Catal. 113 (1988) 144–163.
[37] Y.K. Kao, L. Lei, Y.S. Lin, Catal. Today 82 (2003) 255–273.
[38] P. Costamagna, A. Selimovic, M.D. Borghi, G. Agnew, Chem. Eng. J. 102 (2004) 61–69.
[39] S.M. Ghoreishi, A. Akgerman, Sep. Purif. Technol. 39 (2004) 39–50.
[40] S. Assabumrungrat, T. Rienchalanusarn, P. Praserthdam, S. Goto, Chem. Eng. J. 85 (2002) 69–79.
[41] G. Pipus, I. Plazl, T. Koloini, Chem. Eng. J. 76 (2000) 239–245.
[42] J. Coronas, M. Menendez, J. Santamaria, Ind. Eng. Chem. Res. 34 (1995) 4229.
[43] R. Ramos, M. Menendez, J. Santamaria, Catal. Today 56 (2000) 239–245.
[44] C. Tellez, M. Menendez, J. Santamaria, Chem. Eng. Sci. 54 (1999) 2917–2925.
[45] C. Tellez, M. Menendez, J. Santamaria, AIChE J. 43 (1997) 777.
[46] S. Assabumrungrat, P. Praserthdam, S. Goto, J. Chin. Inst. Chem. Engrs. 31 (2000) 19–25.